

Biochemistry. Author manuscript; available in PMC 2014 February 28.

Published in final edited form as:

Biochemistry. 2010 November 16; 49(45): 9722–9731. doi:10.1021/bi100907m.

Distance Mapping in Proteins Using Fluorescence Spectroscopy: The Tryptophan-Induced Quenching (TrIQ) Method

Steven E. Mansoor^{‡,#}, Mark A. DeWitt^{‡,#}, and David L. Farrens^{‡,*}

[‡]Department of Biochemistry and Molecular Biology, Oregon Health and Science University, Portland, Oregon 97239-3098, USA

Abstract

Studying the interplay between protein structure and function remains a daunting task. Especially lacking are methods for measuring structural changes in real time. Here we report our most recent improvements to a method that can be used to address such questions. This method, which we now call Tryptophan induced quenching (TrIQ), provides a straightforward, sensitive and inexpensive way to address questions of conformational dynamics and short-range protein interactions. Importantly, TrIQ only occurs over relatively short distances (~5 to 15 Å), making it complementary to traditional fluorescence resonance energy transfer (FRET) methods that occur over distances too large for precise studies of protein structure. As implied in the name, TrIQ measures the efficient quenching induced in some fluorophores by tryptophan (Trp). We present here our analysis of the TrIQ effect for five different fluorophores that span a range of sizes and spectral properties. Each probe was attached to four different cysteine residues on T4 lysozyme and the extent of TrIQ caused by a nearby Trp was measured. Our results show that for smaller probes, TrIQ is distance dependent. Moreover, we also demonstrate how TrIQ data can be analyzed to determine the fraction of fluorophores involved in a static, non-fluorescent complex with Trp. Based on this analysis, our study shows that each fluorophore has a different TrIQ profile, or "sphere of quenching", which correlates with its size, rotational flexibility, and the length of attachment linker. This TrIQ-based "sphere of quenching" is unique to every Trp-probe pair and reflects the distance within which one can expect to see the TrIQ effect. It provides a straightforward, readily accessible approach for mapping distances within proteins and monitoring conformational changes using fluorescence spectroscopy.

Site-directed labeling $(SDL)^1$ is a powerful tool for assessing protein structure and monitoring conformational dynamics (1–10). In SDL studies, cysteine residues are

SUPPORTING INFORMATION AVAILABLE

The following further materials are provided in the Supporting Information at http://pubs.acs.org: derivations for the analysis method used to determine the relative fraction of static and dynamic quenching in a TrIQ Study; a table reporting the spectral characteristics of labeled T4 lysozyme samples; a table reporting the thermodynamic characterization of some of the labeled T4 lysozyme samples; a table reporting the susceptibility of the various fluorophores (shown in Figure 1) to quenching in the presence of different amino acids; a table reporting the results from lifetime analysis of the fluorescence decay measurements (used to generate Figures 2B, 3B); and a table of values (used to generate Figure 5A and 5B) that reports the fraction of fluorophores that have either formed a static complex, are dynamically quenched or are unquenched.

¹Abbreviations:

SDL, site-directed labeling; EPR, electron paramagnetic resonance; FRET, fluorescence resonance energy transfer; TrIQ, tryptophan induced quenching; Trp, tryptophan; T4L, T4 lysozyme; PET, photoinduced electron transfer; mBBr, monobromobimane; PDT-Bimane, (2-Pyridyl)dithiobimane; qBBr, monobromotrimethylammoniobimane; LY, lucifer yellow; BDPY, BODIPY 507/545; Atto, Atto-655; Cy5, Cyanine-5.

^{*}To whom correspondence should be addressed. Phone: 503-494-058 farrensd@ohsu.edu Fax: 503-494-8393. #These two authors contributed equally to the initial aspects of this work.

introduced into strategic areas in a protein and labeled with thiol-reactive spin or fluorescent labels. The spectral data from these probes are then analyzed to glean insights into the probe's mobility and solvent accessibility.

Secondary structure in proteins can be identified by carrying out a systematic SDL scan through a sequence, as the compiled data display patterns reflecting the periodicity of an alpha helix or beta strand (11–13). However, SDL methods for studying tertiary structure are much less straightforward, and intense research has gone into developing new SDL-based ways to map distances in biomolecules. Recently, EPR based methods have been developed to measure distances with good precision (14–18). Fluorescence-based SDL methods can also measure distances, and these are usually based on some variation of Förster resonance energy transfer (FRET) (19–25). Unfortunately, except for an exception (26), FRET methods are usually not well-suited for studying small dynamic changes in proteins, or for determining how a secondary structure packs into a tertiary structure. This is because most probes used in FRET are relatively large, 100% labeling efficiency is usually required for the acceptor probe, and most FRET methods are optimized for measuring longer-range distances (~20 – 100 Å).

We have developed a new fluorescent approach for measuring distances within proteins that circumvents most of these problems. We call this approach TrIQ, for Tryptophan induced quenching. TrIQ exploits the dramatic quenching effect that tryptophan (Trp) has on the emission intensity of some fluorophores. TrIQ studies are relatively straightforward to carry out – the protein is labeled with a single fluorophore and then the extent of fluorescence quenching caused by a nearby tryptophan (Trp) residue is measured.

The TrIQ method has a number of unique advantages over other SDL methods. TrIQ primarily occurs only over short distances (5–15 Å), making it ideal for assessing short-range distances and small changes in protein structure. Furthermore, there are several practical advantages inherent to the TrIQ method. These include: i) only one probe is used in a TrIQ study, and thus only one cysteine is labeled, ii) the labeling efficiency does not have to be 100% (since TrIQ monitors the fluorescence of the probe, and the quenching Trp is always present in every protein, under-labeled samples can be studied), iii) it is not necessary to carry out extensive Trp mutations (in fact, native Trp residues can be left remaining in the protein, or even exploited to act as the quencher), iv) TrIQ studies can be carried out using only microgram amounts of sample at low concentrations, v) the instrumentation is simple and widely available, and vi) TrIQ can be adapted for high-throughput applications (13).

We first discovered TrIQ can be used to study protein structure during a systematic study of the fluorescent probe bimane, while it was attached to cysteine mutants of T4 lysozyme (13, 27). The data showed there was substantial TrIQ only when the bimane fluorophore and quenching Trp residue were near van der Waal's contact distance, or more generally, when the C_{α} - C_{α} carbon distance between the cysteine attachment site and the Trp quencher was $\sim 5-15 \ \text{Å}$.

Subsequently, the TrIQ-bimane approach has been used for a wide array of studies. It has been used to identify key sites of conformational change in the G-protein coupled receptors rhodopsin and the beta-adrenergic receptor (28-30), to study the interaction of rhodopsin with the G-protein transducin (31), to orient the interaction between molecular chaperone proteins and their targets (32), to investigate the dynamic structural changes in a cyclic nucleotide-gated ion channel upon activation (33), and to study the secondary structure of the S3-S4 linker of K^+ channels (34).

All of the TrIQ studies referenced above used derivatives of bimane, either monobromobimane (mBBr), a positively charged bimane (qBBr), or PDT-bimane (which attaches through a disulfide linkage). Overall, bimane is an excellent probe for TrIQ studies of protein structure and dynamics, as it is small, non-polar, and has well characterized spectral properties (35–37). However, bimane has some disadvantages, including a relatively low absorbance ($\epsilon_{380~\text{nm}} = 5{,}000~\text{L}~\text{cm}^{-1}~\text{M}^{-1}$), and the need for UV excitation (at ~ 380 nm). These two limitations reduce the sensitivity of TrIQ-bimane and hamper its use in cell-based and *in vivo* imaging studies.

Thus, in the present manuscript, we set out to overcome these limitations, and to significantly expand the TrIQ "toolbox". Our goal was to increase the distance and spectral range over which TrIQ studies can be carried out, and to increase the number of probes that can be used to cross-check distances determined in a TrIQ study. To do this, we measured the distance over which TrIQ occurred for several fluorophores previously identified to be sensitive to Trp-induced quenching (34, 38–41). We carried out these calibrations while these probes were attached to T4 lysozyme (T4L), thus enabling the spectral data to be assessed in the context of a known protein structure. Importantly, several of the probes can be used for cell based imaging studies, thus opening the possibility of carrying out TrIQ studies in a whole cell environment

We also present a comprehensive analytical method for analyzing TrIQ data. This analysis, which is simple in execution, can be used to identify where and quantify how many Trp/fluorophore pairs have formed non-fluorescent complexes at the moment of light excitation. This concept can be used to determine a "sphere of static quenching" for each probe, which defines the distance within which the probe can form a static complex with a Trp residue. Since these complexes form before (or during) the subnanosecond process of light absorption by the fluorophore, their presence gives direct, unambiguous evidence that two parts of a protein are in very close proximity, with subnanosecond timescale resolution. We propose measuring the formation of these complexes provides a unique and powerful tool for mapping protein distances, monitoring dynamic changes in proteins, and detecting shifts in conformational equilibria.

MATERIALS and METHODS

Materials

Unless otherwise noted, all basic reagents and biochemical supplies (buffers, salts, concentrators, plastic-ware, etc.) were purchased from Fisher or Sigma and their affiliates. The Tris base and ultrapure guanidine HCl were purchased from Invitrogen (Carlsbad, CA), the fluorescent probe qBBr was purchased from Toronto Research Chemicals (North York, Ontario, Canada) and BODIPY 507/545 iodoacetamide and Lucifer Yellow iodoacetamide were purchased from Molecular Probes (Eugene, OR). Cy5-maleimide was purchased from GE Healthcare. Atto-655 maleimide was purchased from Atto-tec (Siegen, Germany).

Buffers

The buffers used were as follows: buffer A, 50 mM MOPS, 50 mM Tris, and 1 mM EDTA, pH 7.6; buffer B, 20 mM Tris, 20 mM MOPS, 0.02% sodium azide, 1 mM EDTA, and 1 mM DTT, pH 7.6; buffer C, 20 mM KH₂PO4 and 25 mM KCl, pH 3.00; buffer D, 25 mM MOPS, 25 mM Tris, 1 mM EDTA, pH 7.6, and 3 M guanidine hydrochloride; Buffer E, 250 mM MOPS, 250 mM Tris, 1 mM EDTA, pH 7.6; Buffer F, 12 g tryptone digest, 5 g yeast extract, 10 g NaCl, 1 g glucose, 1 mL 100 mg/mL ampicillin per liter of medium.

Nomenclature

Throughout the paper, mutants are named by specifying the original residue, the number of the residue, and the new residue, in that order. Thus, for example, the code N132C indicates that the native asparagine residue at the 132^{nd} amino acid position was mutated to a cysteine. Similarly, N116W indicates the native asparagine was mutated to a tryptophan. For labeled mutant samples, each fluorophore has its own suffix: $-B_1$ for monobromobimane, -qBBr for monobromotrimethylammoniobimane, -LY for lucifer yellow, -BDPY for BODIPY, -Atto for Atto-655, and -Cy5 for Cyanine-5. Thus, for example, the name N132-qBBr indicates that the native asparagine residue at the 132^{nd} amino acid position has been mutated to a cysteine and reacted with the qBBr label.

Construction, Expression and Purification of T4 Lysozyme Mutants

The construction of the T4L cysteine mutants used in the present work has been previously described (27, 37). Briefly, K38 *Escherichia coli* cells were transformed with the T4L cysteine-mutant plasmid and inoculated into 25 mL of buffer F and grown overnight with shaking. The next morning, 10-15 mL of overnight growth were added to 500 mL of buffer F in a 2.8 L flask, and grown with 250 rpm shaking at 37 °C. Protein production was induced in late log phase cultures (OD₆₀₀ of ~1.2) by the addition of IPTG to a final concentration of 1 mM. The induced cultures were allowed to express for 1.5-2 hours at room temperature until harvesting by centrifugation. Pelleted cultures were stored at -80 °C for later use.

Mutant T4L was purified using cation exchange chromatography with a slight modification of a previously described protocol (13, 27, 37). Briefly, thawed pellets containing expressed mutant lysozyme were resuspended manually in 30-35 mL Buffer B, lysed, and cleared by centrifugation at $10,000 \times g$ for 30 minutes. DTT was added to ~20 mM, and the lysate was filtered (0.45 μ m filter) and loaded onto a cation exchange column (GE Healthcare HiTrap, 1 mL SP Sepharose) pre-equilibrated with buffer A. The samples were eluted with a salt gradient in buffer A (ramped from 0 to 1 M NaCl), over ~1.5 h. T4 lysozyme, eluted at around 200 – 300 mM NaCl, was collected in multiple fractions, snap-frozen in liquid nitrogen, and stored at -80 °C. The purity of the fractions was assessed by SDS-PAGE and judged to be at least 90% pure for all samples studied.

Fluorescence Labeling of T4L Mutants

The fluorophores studied possess a variety of reactive groups and a range of solubilities, thus the method of labeling T4 lysozyme differed slightly with each fluorophore. In general, labeling of ~10 nanomoles of each lysozyme mutant (~100 μM T4L concentration) was carried out using ~ 5 – 10x molar excess of fluorescent label (5x for BODIPY and Lucifer Yellow, 7x for Cy5 maleimide, 10x for Atto-655 maleimide and qBBr), taken from stock solutions made in DMSO. Labeling was carried out in buffer D at 4 °C overnight with gentle agitation. Care was taken to ensure that DMSO concentrations were always 10% of final reaction volume. Labeled protein was separated from free, unreacted label using size-exclusion chromatography. It should be noted that BDPY appeared to induce a small amount of protein aggregation under some conditions, perhaps due to its hydrophobic nature.

For the fluorophores with a maleimide reactive group (Atto-655 and CY5), 1M MOPS was added to lower the pH to ~ 6.5 to avoid amine reactivity and maleimide ring opening. For the BODIPY 507/545 reactions, DMSO was added to a final concentration of 10% to help improve solubility of the relatively insoluble free label. The reactions were then incubated overnight with rocking at 4 $^{\circ}$ C in the dark. For qBBr, unreacted free label was separated from the labeled protein by gel filtration on a desalting column (Pharmacia Biotech HiTrap, 5 mL) equilibrated with buffer A. For all other labels, free label was removed from the

reaction solution by first concentrating the entire reaction to 100 μ L using a 3K MWCO spin concentrator (Amicon Microcon) and then removing free label using G-15 Sephadex in a small desalting column (1.25 cm \times 3 cm) with buffer A and gravity flow. Several sequential passes (1 for BODIPY, 2–3 for LY and Atto, 3–5 for Cy5) and concentration steps over the desalting column were often necessary to ensure adequate separation and removal of free label. Absorption spectra (using a Shimadzu UV 1601) were used to calculate the labeling efficiency for each mutant.

Concentrations were calculated using extinction coefficients of $\epsilon_{280} = 23,327 \text{ L cm}^{-1} \text{ mol}^{-1}$ for T4 lysozyme. For mutants with the N116W mutation, an extinction coefficient value of $\epsilon_{280} = 5600 \text{ L cm}^{-1} \text{ mol}^{-1}$ was added to the WT T4 lysozyme extinction coefficient. The amount of label attached to the protein was approximated using the appropriate extinction coefficient for each label ($\epsilon_{380} = 5,000 \text{ L cm}^{-1} \text{ M}^{-1}$ for mBBr and qBBr; $\epsilon_{508} = 64,000 \text{ L cm}^{-1} \text{ M}^{-1}$ for BODIPY; $\epsilon_{427} = 11,000 \text{ L cm}^{-1} \text{ M}^{-1}$ for Lucifer Yellow; $\epsilon_{655} = 125,000 \text{ L cm}^{-1} \text{ M}^{-1}$ for Atto-655; $\epsilon_{650} = 250,000 \text{ L cm}^{-1} \text{ M}^{-1}$ for Cy5). The contribution from each label at 280 nm was subtracted before calculating protein concentration.

All reacted T4 lysozyme mutants were analyzed by SDS-PAGE for purity and determined to be > 90% pure. Levels of unreacted free label in the samples for all labels (except Atto-655) were determined using a TCA precipitation protocol, as described previously (13). For Atto-655-labeled samples, the absorbance of the sample before addition of TCA was compared to absorbance of the sample after centrifugation. This approach was used because Atto-655 is nonflourescent in acid but we assumed it to have a largely matrix-independent extinction coefficient, based on control experiments with a mercaptoethanol adduct of the free label. In all cases, the amount of signal retained following acid precipitation and centrifugation was taken to be due to unreacted free label. This was < 3% for all samples tested, except for the Cy5-labeled negative control, which was $\sim 10\%$ or less in all cases.

Assessment of Fluorophore Quenching by Free Amino Acids

The protocol for assessing the quenching of the fluorophores by free amino acids was adopted from previous work (42). Measurements were performed using a PTI steady-state fluorimeter, with 1 nm excitation slits (3 nm for qBBr), and 3 nm emission slits. Amino acids were made up to 60 mM stock concentrations in Buffer E. Note that since tyrosine is only minimally soluble in this buffer, the tyrosine methyl ester derivative was used. For the quenching experiments, fluorophores were used at a range of concentrations between 1–10 µM in buffer E. Unquenched intensity was taken as the buffer-subtracted integrated fluorescence of the fluorophore stock diluted 1:1 with buffer E. Quenched intensity was taken as the buffer-subtracted integrated fluorescence of the same fluorophore stock diluted 1:1 with 60 mM amino acid stock (50 mM for tryptophan diluted to 30 mM final concentration) in Buffer E. The ratio of the fluorescence intensity in the presence of quencher (30 mM amino acid) to the fluorescence intensity in the absence of quencher is reported as the relative quantum yield in the presence of the amino acid.

Characterization of Thermodynamic Stability of T4L Mutants

To assess the effect of the different probes on protein stability, we subjected a subset of labeled mutants in buffer C (pH 3.00) to increasing temperatures while monitoring the decrease in a-helical CD signal at 222 nm (43). Mutants E128C and N116W/E128C were chosen for these studies, as our previous work indicated these sites would likely be the most destabilized after label attachment (13, 27, 37). The thermal stability of the labeled mutants was assessed as follows. T4L-fluorophore samples (\sim 500 μ L of \sim 10 μ M protein) were thawed and dialyzed at 4 $^{\circ}$ C overnight against 500 mL \sim 1000 mL of buffer C (pH 3.00) with at least three changes of reservoir in a 3,000 MWCO Slide-A-Lyzer cassette (Pierce

Scientific). The thermal unfolding was monitored at 222 nm using circular dichroism (CD) on an AVIV 215 spectrometer with ~ 350 μL of each sample at concentrations between 3.5 μM – 6 μM . Slit widths were 1 nm. The samples were monitored while heating from 5 to 85 °C, and then cooled to 5 °C and heated again to determine the extent of protein refolding. The labeled samples exhibited greater than 75% refolding, as judged by the recovery of the initial CD signal. Differences in stability between mutant samples were judged from changes in $\Delta\Delta G$, calculated using the approximation that $\Delta\Delta G$ = $\Delta m*\Delta S_{WT}$ (44).

Steady-State Fluorescence and Anisotropy Measurements

All steady-state fluorescence excitation, emission, and anisotropy measurements were carried out using a PTI fluorescence spectrometer in a T-format at room temperature. The parameters of the fluorescence emission spectra were measured as follows. <u>T4L-qBBr</u>: 380 nm excitation, 395 – 600 nm emission, 2 μ M sample, 1 nm exc. slits, 10 nm emission slits; <u>T4L-BDPY</u>: 490 nm excitation, 495 – 750 nm emission, 1.5 – 2.5 μ M sample, 1 nm excitation slits, 3 nm emission slits; <u>T4L-LY</u>: 427 nm excitation, 432 – 750 nm emission, 2 – 3 μ M sample, 1 nm excitation slits, 3 nm emission slits; <u>T4L-Atto</u>: 620 nm excitation, 625 – 900 nm emission, 0.7 – 1 μ M labeled sample, 1 nm excitation slits, 3 nm emission slits; <u>T4L-Cy5</u>: 615 nm excitation, 620 – 850 nm emission, 0.3 – 0.5 μ M sample, 1 nm excitation slits, 3 nm emission slits.

The parameters for the fluorescence excitation spectra were measured as follows: $\underline{T4L}$ \underline{qBBr} : 300-450 nm excitation scan, 490 nm emission, $2~\mu M$ sample, 1 nm exc. slits, 5 nm emission slits; $\underline{T4L}$ -BDPY: 250-530 nm excitation scan, 535 nm emission, $1.5-2.5~\mu M$ sample, 1 nm excitation slits, 3 nm emission slits; $\underline{T4L}$ -LY: 240-520 nm excitation scan, 530 nm emission, $2-3~\mu M$ sample, 1 nm excitation slits, 3 nm emission slits; $\underline{T4L}$ -Atto: 250-675 nm excitation, 680 nm emission, $0.7-1~\mu M$ labeled sample, 1 nm excitation slits, 3 nm emission slits; $\underline{T4L}$ -Cy5: 615 nm excitation, 620-850 nm emission, $0.3-0.5~\mu M$ sample, 1 nm excitation slits, 3 nm emission slits, 3 nm emission slits, 3 nm emission slits,

Anisotropy measurements were carried out at 22 °C using the labeled T4L samples at the above concentrations in buffer A. Excitation light was polarized vertically and emission light collected simultaneously using vertical and horizontal polarization of the two emission monochromators in the T-format spectrofluorimeter. G-factors for each sample were calculated using a horizontally polarized excitation beam. Excitation/emission parameters (in nm) for each set of labeled samples were taken at the excitation/emission maxima for each fluorophore: 381/475 for T4L-qBBr; 506/530 for T4L-BDPY; 427/525 for T4L-LY; 664/678 for T4L-Atto, and 650/665 for T4L-Cy5. For all samples, excitation slits were set at 3 nm and emission slits were 5 nm. The measurements were performed in duplicate and the average steady-state anisotropy was obtained using buffer subtraction of individual intensities and real-time emission and excitation correction.

Interestingly, significant amounts of BDPY-labeled sample were lost upon repeated pipetting, so pipetting was kept to a minimum when handling these samples.

Quantum Yield Measurements

The quantum yield of each labeled mutant was measured using quinine sulfate as the standard (quantum yield of 0.55 in $1~N~H_2SO_4$), except for mutants labeled with Atto-655 and Cy5, for which rhodamine 6G was used as a standard (quantum yield of 0.94 in ethanol). For the red-shifted fluorophores (BODIPY, Atto-655, and Cy5), emission correction was used to account for drop-off of photomultiplier tube sensitivity at longer wavelengths. Measurements involved matching the absorbance maximum of the standard to each of the labeled T4 lysozyme samples and measuring integrated fluorescence emission

intensity under identical optical conditions (350 nm excitation, 355 - 750 nm emission for the quinine sulfate standard; 500 nm excitation, 505 - 750 nm emission for the rhodamine standard). In all cases, the buffer intensity was subtracted before integrating the fluorescence intensity.

Fluorescence Lifetime Measurements

Fluorescence lifetimes for all the samples (except those labeled with BODIPY) were measured at 22 $^{\circ}$ C using a PTI Laserstrobe fluorescence lifetime instrument at sample concentrations identical to those used for the steady-state measurements (see above). The lifetimes for the BODIPY-labeled samples were measured at room temperature using the PTI EasyLife system, with excitation from a 505 nm LED and emission collected using longpass filters. For all lifetime measurements, the instrument response function (IRF ~ 1.5 ns) was determined using a solution of Ludox.

Experiments were set up to ensure < 5% measured intensity due to scattered light using the following parameters for each fluorophore set. $\underline{T4L\text{-}qBBr}$: measurements used 381 nm excitation passed through a 298 – 435 nm band-pass filter, and emission was monitored through two long-pass filters (> 470 nm). Each lifetime decay was measured using two averages of five shots per point, collected randomly in time over 150 channels; $\underline{T4L\text{-}BDPY}$: Measurements used a 500 nm interference filter on excitation from a 505 nm LED, and emission was collected using two > 520 nm plus one > 550 nm longpass filters on emission. Each lifetime decay was measured using three averages of 150 data points collected randomly in time; $\underline{T4L\text{-}LY}$: Measurements used 427 nm excitation and emission collected on a monochromator at 527 nm (6 nm slits) plus two > 500 nm longpass filters. Each decay was measured using two averages of 400 data points collected randomly in time; $\underline{T4L\text{-}Atto}$: Measurements used 640 nm excitation and emission was collected at 676 nm emission (6 nm slits). Each lifetime decay was measured using two averages of 300 data points collected randomly in time using PTI software.

Data were acquired using an arithmetic data collection method, and analyzed using the commercial PTI T-Master software with either single exponential or double exponential fits. Goodness of fit was evaluated by χ^2 values (acceptable values between 0.8 and 1.2) and visual inspection of the residuals.

Integrated Steady-State Fluorescence Intensities

Integrated steady-state fluorescence intensities were calculated from the steady-state fluorescence emission scans of each labeled sample. The integrated fluorescence intensities with (F_w) and without (F_0) the presence of the tryptophan at residue 116 were used to calculate the amount of static complex formation (see below). The following integration parameters were used for each fluorophore-labeled sample: $\underline{T4L\text{-mBBr}}$: integration from 410 nm to 600 nm; $\underline{T4L\text{-qBBr}}$: integration from 495 nm to 750 nm; $\underline{T4L\text{-LY}}$: integration from 435 to 750 nm. $\underline{T4L\text{-Atto}}$: integration from 625 nm to 800 nm.

Calculation of Static Complex Formation

The fraction of static, pre-formed complex $(1-\gamma)$ between each Trp/fluorophore pair was calculated as described by Spencer and Weber for measuring the amount of static and dynamic intra-molecular quenching in a linked fluorophore and quencher pair. A brief description of the analysis is provided in the Discussion, and a full derivation of γ can be found in the Supporting Information.

RESULTS and DISCUSSION

Overview of Experiments

Figure 1A shows the sites of fluorophore attachment on the protein and the relevant C_{α} - C_{α} distances from each cysteine residue to the quenching Trp. Figure 1B shows each probe drawn on the same scale, with the respective absorbance and emission wavelength maxima (the full spectra are given in Supporting Figure 1). Throughout the text we refer to these probes using the following abbreviations: monobromobimane (mBBr)², monobromotrimethylammoniobimane (qBBr, a positively charged bimane derivative), lucifer yellow (LY), BODIPY 507/545 (BDPY), and Atto-655 (Atto)³. Cyanine-5 (Cy5) was also studied as a negative control.

Characteristics of the Labeled Mutants

The purification, labeling and characterization of the T4 lysozyme cysteine mutants are detailed in the Supporting Information. As listed in Supporting Table 1, typical labeling efficiencies were greater than 80%, and ranged from 50% to 100% (as noted in the introduction, TrIQ studies can be carried out on samples that are not quantitatively labeled). The amount of free fluorescent label was < 3% in all mutants tested, and none of the fluorophores showed significant background labeling for a cys-less wild-type T4L. Our thermodynamic stability assays showed that most of the probes do not substantially decrease T4L stability ($\Delta\Delta G$ values of -0.8 kcal/mole), although not surprisingly, the largest probe, Atto-655, did show increased destabilization ($\Delta\Delta G$ value of -1.6 kcal/mole). The results of these stability assays are reported in Supporting Table 2. In general, the Trp residue at site 116 did not affect the labels' anisotropy, or the lambda max for excitation or emission. However, changes in the absorbance λ_{max} values were observed at several sites (see Supporting Table 1), indicating some perturbation of the probe in the ground state (discussed further below).

The Fluorescence Intensity Depends on the Distance of the Probe from the Trp, but the Fluorescence Lifetime Does Not

We confirmed that the fluorophores used in this study are susceptible to tryptophan-induced quenching by carrying out studies of the free probes and tryptophan together in solution (Supporting Table 3). The effect of the Trp quencher on the emission intensity of each label was compared as follows. First, for each Trp/probe pair, the samples were matched to ensure that the same amount of label was present in the samples containing the Trp at site 116 (N116W) and those without (N116). Then, the steady-state fluorescence emission intensity was measured. These data are reported in Figure 2A. Comparing the emission intensities shows that for all of the probes except Atto 655, the TrIQ effect (the decrease in fluorescence intensity) depends on how far the probes is from the Trp at 116 (Figure 2A). However, the absolute amount of quenching clearly varies for different fluorophores, presumably because of differences in probe size, linker length, etc. Interestingly, the Trp quenching of LY and Atto was substantial and occurred at all sites tested. Note - the fluorophore Cy5 was tested as a negative control and it showed little quenching by Trp (data not shown).

²The tryptophan-induced fluorescence quenching data of mBBr has been reported earlier (Ref. 27) but it has not previously been subjected to the new analysis method we present here. Thus, we have included the analysis of the previous mBBr data to further demonstrate the utility of the TrIQ method.

The Atto structure was inferred based on patent USPTO # 2006/0179585 A1, and the molecular weight and fluorescence properties

were obtained from the manufacturer.

It is not possible to precisely define all the reasons for the observed differences in the amount of quenching for each Trp/fluorophore pair at each site, because the photo-induced electron transfer (PET) quenching mechanism is affected by a number of difficult to experimentally define variables. These variables include the local solvent polarity at the site of attachment, and the shape and relative orientation of the two molecule pairs (45–46). These factors are for the most part unknown and will vary for each of the different fluorophore/Trp pairs discussed here. For these reasons, as discussed further below, we developed an empirical approach for assessing the proximity of each fluorophore to the Trp. This approach compares the steady-state fluorescence data with the rates of fluorescence decay, and uses these values to define a "sphere of quenching" (the distance within which one will observe measurable quenching) for each probe/Trp pair. As discussed below, the "sphere of quenching" can be even further defined and quantified to provide further distance information.

Fluorescence lifetimes were thus next measured to determine if the rate of fluorescence decay would change in a distance-dependent way. These data were fit with either mono- or bi-exponential decays and are reported in Supporting Table 4. To enable comparison with the steady-state intensity data (47), the lifetime data are also plotted in Figure 2B as $<\tau>$, the amplitude-weighted fluorescence lifetime⁴. Although the lifetime data show changes in the presence of the Trp quencher, it is clear that the magnitude of these changes in $<\tau>$ do not mirror the changes in intensity and are not strictly dependent on the distance of the label from the Trp for all of the probes.

We further assessed the distance dependence of TrIQ by plotting the ratio of the emission or lifetime data (with and without the Trp quencher) vs. the separation distance from the Trp (Figure 3). In order to test this relationship further, the analysis of the mBBr samples included data from three other Trp/mBBr pairs we reported in our previous study (27). The ratio data clearly show that the TrIQ effect on emission intensity depends on the distance of the label from the Trp quencher at site 116 (Figure 3A). In all cases except Atto, the greatest quenching of emission intensity occurs for C_α - C_α distances 10 Å. Interestingly, these ratio plots also highlight the discrepancy between the Trp-induced changes in fluorescence emission intensity (F_0 / F_w) and the fluorescence lifetime ($<\tau_0>$ / $<\tau_w>$) data. Unlike the TrIQ effect on emission intensity (Fig. 3A), the TrIQ effect on fluorescence lifetime does not appear to correlate with distance (Fig. 3B). This result is extremely informative, because in the absence of other quenching effects, the plots of the TrIQ effect on emission intensity (F_0 / F_w) and fluorescence lifetime ($<\tau_0>$ / $<\tau_w>$) should be the same (47). The fact that they are not indicates other processes are occurring besides dynamic quenching, and the nature of processes can be analyzed to yield further distance constraints for the data.

The presence of non-fluorescent, Trp-fluorophore complexes is indicated by differences in the extent of fluorescence intensity quenching vs. fluorescence lifetime quenching

Roughly speaking, a probe can undergo three possible fates after light excitation in a TrIQ study. One possibility is the probe is too far away to interact with the Trp, and thus is not quenched (Figure 4, top). A group of these fluorophores would appear as if there was no Trp present, and thus show no change in the fluorescence intensity or lifetime. A second possibility is that the probe is "dynamically quenched" by the Trp residue (Figure 4, middle). Dynamic quenching means that, at some time after absorbing a photon (yet while still in the excited state), the probe becomes close enough to interact with the Trp and thus is quenched. Each Trp-probe has a unique "sphere of dynamic quenching", the radius of which

⁴The value of $<\tau>$ is the amplitude-weighted fluorescence lifetime, defined as: $<\tau>=\Sigma\alpha_i\tau_i$, where α_i is the normalized pre-exponential factor for each lifetime, τ_i .

reflects the distance within which dynamic quenching can occur. A group of dynamically-quenched fluorophores exhibit both decreased fluorescence intensity and a shorter fluorescence lifetime. Thus, with pure dynamic quenching, $F_0/F_w = <\tau_0>/<\tau_w>$. Finally, the probe could be "statically quenched". In static-quenching, the probe is in a complex with the Trp even before light absorption (Figure 4, bottom). Statically-quenched complexes are non-fluorescent, thus they do not contribute to the observed emission intensity, and have no effect on the observed rate of fluorescence decay (fluorescence lifetime). Similarly, each Trp-probe pair has a unique "sphere of static quenching", which reflects the distance within which the Trp and probe are close enough to physically interact to form a ground-state complex resulting in static quenching. When static quenching is present, $F_0/F_w <<\tau_0>/<\tau_w>$ and F_0/F_w is greater than $<\tau_0>/<\tau_w>$.

This simple model illustrates how in TrIQ, the different ways the photo-excited probe can interact with the Trp contribute differently to the overall observed fluorescence intensity and lifetime. To reiterate, both dynamic and static quenching decrease the fluorescence emission intensity one observes for a sample, but only dynamic quenching effects the fluorescence lifetime - static quenching does not. Thus, changes in the fluorescence lifetime only reflect the unquenched and dynamically quenched probes.

Thus, it is simple to determine if "static quenching" is occurring in a TrIQ study -one simply compares the intensity and lifetime of a sample in the presence and absence of the Trp quencher. If the change in the amplitude-weighted fluorescence lifetime ratio in the presence of Trp ($<\tau_0>/<\tau_w>$) is less than the change in fluorescence intensity ratio (F0/Fw), then some of the probes in the sample are undergoing static quenching.

Based on this type of analysis, one can see that the data in Figure 3 indicate many of the samples have significant non-fluorescent, static complexes present. In particular, the LY and Atto-labeled mutant pairs showed dramatic TrIQ effects on the fluorescence intensity, yet little to no change in fluorescence lifetime. These discrepancies, as well as the observed shifts in absorbance λ_{max} values (Supporting Table 1) indicate ground-state interactions and "static quenching" for many of the fluorophore/Trp pairs.

The presence of a Trp-Fluorophore complex provides direct evidence of close proximity

For the probes we used in this study, the Trp-induced quenching mechanism is thought to involve photoinduced electron transfer, or PET (34, 38–40). Unfortunately, it is not possible to calculate distances between Trp/fluorophore pairs using PET theory alone, because although PET efficiency does depend on distance, it also depends on a number of unknown variables, such as steric and stereochemical factors of the probes and the local dielectric constant. However, we realized there is a simple way to assess fluorophore-Trp distances in TrIQ studies – by quantifying the amount of static complex formation (discussed above). After all, two molecules close enough to form a non-fluorescent, static complex are, by definition, "very close".

The amount of Trp-Fluorophore complex can be quantified

In TrIQ, the fluorophore and quencher are both attached to the same molecule. Thus, the quenching is intra-molecular and concentration-independent. We discovered the fraction of static quenching in TrIQ data can be calculated by applying an approach originally developed by Gregorio Weber and his graduate student Richard Spencer to assess intra-molecular quenching in FAD and NADH (48, 49). A brief explanation of this analysis is given below, and more detail is provided in the Supporting Information.

To quantify the relative fraction of Trp/fluorophore complexes present in a TrIQ study, one first uses the fluorescence data to calculate γ , the fraction of total fluorophores that absorb a photon but are not in a static-complex with the Trp. Mathematically, γ is defined as:

$$\gamma = \left(\frac{F_w}{F_0}\right) \left(\frac{\tau_0}{\tau_w}\right)$$

where F_w and τ_w represent the relative fluorescence intensity (or quantum yield) and fluorescence lifetime of the fluorophore in the presence of the Trp quencher. F_0 and τ_0 represent the relative fluorescence intensity (quantum yield) and fluorescence lifetime in the absence of the Trp quencher. Once γ has been determined, it is simple to determine the relative fraction of fluorophores in a non-fluorescent, static complex - it is (1 - $\gamma)$. Note - in this analysis, any ultra-fast dynamic quenching events that are too fast to be measured by the fluorescence lifetime instrument (in our case, less than $\sim 200~ps)$ will end up being interpreted as "static quenching. See the Supporting Information for a complete description of these calculations and relationships."

The amount of Trp-fluorophore static complex formation provides distance constraints for the TrIQ data

A striking result is observed when static complex formation is plotted as a function of distance from the Trp - there is a clear distance dependence as well as variation between probes (Figure 5A). These differences define the "sphere of static quenching" for each probe, which correlates extremely well with the sizes of each probe and its attachment linker (compare probe size in Figure 1B with degree of static quenching in Figure 5A). For example, mBBr only shows substantial static-quenching at distances less than 10 Å, and it shows no static complex formation for C_{α} - C_{α} distances at or greater than 10 Å. Hence, for mBBr, the "sphere of static quenching" is within 10 Å. The qBBr and BDPY probes have some static quenching over a slightly broader distance range (~40–50% static complex for C_{α} - C_{α} distance of 10 Å), but they only show dynamic quenching at the longer C_{α} - C_{α} distances. In contrast, most of the quenching for the larger LY and Atto 655 probes occurs through static, non-fluorescent complexes over the entire range of distances we studied here. Calculations of the relative fractions of static quenching, dynamic quenching, and unquenched fluorescence for each probe is reported in Supporting Table 5, and graphically displayed in Figure 5B.

The TrIQ properties of each probe are not identical - each probe has different advantages and disadvantages

Our results clearly show how the behavior of each probe must be considered when designing a TrIQ study. For example, mBBr has the most discriminating "sphere of quenching" - it only exhibits static complex formation for C_{α} - C_{α} distances < 10 Å. Probe qBBr, which is similar in structure and behavior to mBBr, shows significant static complex formation out to 10 Å. This might be due to the extra length added by the permanent positive charge in qBBr, which also renders it less able to penetrate a biological membrane, thus making it potentially useful for specifically labeling extracellular cysteine residues.

Like the bimanes, BDPY is a small probe that shows primarily static complex formation for distances $10~\mbox{Å}.$ BDPY has an advantage of being highly absorptive ($\epsilon_{508}=64,\!000~\mbox{L}~\mbox{cm}^{-1}$ M^{-1}) and having a good quantum yield ($\Phi\sim0.4$). Most importantly, BDPY is significantly red-shifted (maximum absorbance at 508 nm), which should enable it to be used in biological tissue with less background absorbance.

LY and Atto were the two largest fluorophores in our study. Perhaps due to their size and/or the flexibility of their linkers, both showed primarily static complex formation for all the sites studied, even at fluorophore/quenching distances up to 11 Å. We feel these two probes are thus not suitable for precisely discriminating small-scale intramolecular distances within proteins. However, each probe would be beneficial in a TrIQ study designed to assess intermolecular protein-protein interactions, or other studies in which a simple binary change in signal is sufficient. Furthermore, the high extinction coefficient, large quantum yields, and ability to be excited and monitored at visible wavelengths, makes both LY and Atto much more attractive for use in imaging and *in-vivo* applications.

CONCLUSIONS

In the present work, we expanded the palette of probes for the TrIQ method, and we introduced a new, comprehensive approach for analyzing TrIQ data. Our results show a different "sphere of quenching" for different probes, and these must be considered when designing a TrIQ study. Experiments requiring short-range distance resolution, such as detecting local conformational changes in a protein, will be best pursued using probes with a smaller "sphere of quenching", such as mBBr, qBBr or BDPY. In contrast, experiments which can forgo short distance resolution in exchange for a more robust or "binary" signal of "close" versus "not close" (such as assessing protein/protein interactions, drug screening assays or large-scale structural rearrangements in protein complexes) will be better off using probes with a larger "sphere of quenching" like LY or Atto 655. Perhaps most compelling is the prospect of carrying out comprehensive TrIQ studies using combinations of the probes described here, in order to achieve maximal distance resolution.

Supplementary Material

Refer to Web version on PubMed Central for supplementary material.

Acknowledgments

We thank Eric Gouaux (HHMI, Vollum Institute, OHSU) and Arthur Glasfeld (Reed College) among others for critical reading of this manuscript.

This work was supported in part, by National Institutes of Health grants DA018169 and EY015436 (to D.L.F.). S.E.M. was supported in part by research fellowships from F30DA15584.

REFERENCES

- Kaback HR, Sahin-Toth M, Weinglass AB. The kamikaze approach to membrane transport. Nat Rev Mol Cell Biol. 2001; 2:610–620. [PubMed: 11483994]
- Thomas DD, Kast D, Korman VL. Site-directed spectroscopic probes of actomyosin structural dynamics. Annu Rev Biophys. 2009; 38:347–369. [PubMed: 19416073]
- 3. Hubbell WL, McHaourab HS, Altenbach C, Lietzow MA. Watching proteins move using site-directed spin labeling. Structure. 1996; 4:779–783. [PubMed: 8805569]
- Kachel K, Ren J, Collier RJ, London E. Identifying transmembrane states and defining the membrane insertion boundaries of hydrophobic helices in membrane-inserted diphtheria toxin T domain. J Biol Chem. 1998; 273:22950–22956. [PubMed: 9722516]
- Gether U, Lin S, Kobilka BK. Fluorescent labeling of purified beta 2 adrenergic receptor. Evidence for ligand-specific conformational changes. J Biol Chem. 1995; 270:28268–28275. [PubMed: 7499324]
- 6. Venezia CF, Meany BJ, Braz VA, Barkley MD. Kinetics of association and dissociation of HIV-1 reverse transcriptase subunits. Biochemistry. 2009; 48:9084–9093. [PubMed: 19715314]

7. Klare JP, Bordignon E, Doebber M, Fitter J, Kriegsmann J, Chizhov I, Steinhoff HJ, Engelhard M. Effects of solubilization on the structure and function of the sensory rhodopsin II/transducer complex. J Mol Biol. 2006; 356:1207–1221. [PubMed: 16410012]

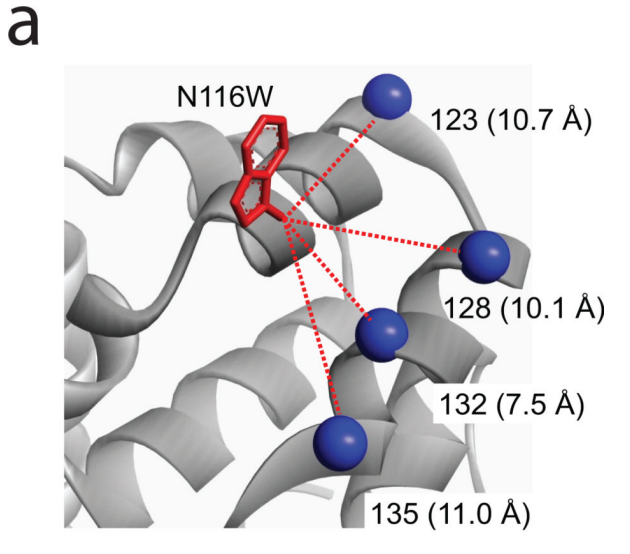
- 8. Kim TY, Uji-i H, Moller M, Muls B, Hofkens J, Alexiev U. Monitoring the interaction of a single G-protein key binding site with rhodopsin disk membranes upon light activation. Biochemistry. 2009; 48:3801–3803. [PubMed: 19301833]
- Hoersch D, Otto H, Wallat I, Heyn MP. Monitoring the conformational changes of photoactivated rhodopsin from microseconds to seconds by transient fluorescence spectroscopy. Biochemistry. 2008; 47:11518–11527. [PubMed: 18847221]
- Yang CS, Sineshchekov O, Spudich EN, Spudich JL. The cytoplasmic membrane-proximal domain of the HtrII transducer interacts with the E-F loop of photoactivated Natronomonas pharaonis sensory rhodopsin II. J Biol Chem. 2004; 279:42970–42976. [PubMed: 15262967]
- 11. McHaourab HS, Berengian AR, Koteiche HA. Site-directed spin-labeling study of the structure and subunit interactions along a conserved sequence in the alpha-crystallin domain of heat-shock protein 27. Evidence of a conserved subunit interface. Biochemistry. 1997; 36:14627–14634. [PubMed: 9398181]
- 12. Perozo E, Cortes DM, Cuello LG. Three-dimensional architecture and gating mechanism of a K+channel studied by EPR spectroscopy. Nat Struct Biol. 1998; 5:459–469. [PubMed: 9628484]
- 13. Mansoor SE, Farrens DL. High-throughput protein structural analysis using site-directed fluorescence labeling and the bimane derivative (2-pyridyl)dithiobimane. Biochemistry. 2004; 43:9426–9438. [PubMed: 15260485]
- 14. Rabenstein MD, Shin YK. Determination of the distance between two spin labels attached to a macromolecule. Proc Natl Acad Sci U S A. 1995; 92:8239–8243. [PubMed: 7667275]
- McHaourab HS, Oh KJ, Fang CJ, Hubbell WL. Conformation of T4 lysozyme in solution. Hingebending motion and the substrate-induced conformational transition studied by site-directed spin labeling. Biochemistry. 1997; 36:307–316. [PubMed: 9003182]
- Borbat PP, McHaourab HS, Freed JH. Protein structure determination using long-distance constraints from double-quantum coherence ESR: study of T4 lysozyme. J Am Chem Soc. 2002; 124:5304–5314. [PubMed: 11996571]
- Sale K, Song L, Liu YS, Perozo E, Fajer P. Explicit treatment of spin labels in modeling of distance constraints from dipolar EPR and DEER. J Am Chem Soc. 2005; 127:9334–9335.
 [PubMed: 15984837]
- Altenbach C, Kusnetzow AK, Ernst OP, Hofmann KP, Hubbell WL. High-resolution distance mapping in rhodopsin reveals the pattern of helix movement due to activation. Proc Natl Acad Sci U S A. 2008; 105:7439–7444. [PubMed: 18490656]
- Stryer L. Fluorescence energy transfer as a spectroscopic ruler. Annu Rev Biochem. 1978; 47:819– 846. [PubMed: 354506]
- Blackman SM, Piston DW, Beth AH. Oligomeric state of human erythrocyte band 3 measured by fluorescence resonance energy homotransfer. Biophys J. 1998; 75:1117–1130. [PubMed: 9675213]
- 21. Bergstrom F, Hagglof P, Karolin J, Ny T, Johansson LB. The use of site-directed fluorophore labeling and donor-donor energy migration to investigate solution structure and dynamics in proteins. Proc Natl Acad Sci U S A. 1999; 96:12477–12481. [PubMed: 10535947]
- 22. Cha A, Snyder GE, Selvin PR, Bezanilla F. Atomic scale movement of the voltage-sensing region in a potassium channel measured via spectroscopy. Nature. 1999; 402:809–813. [PubMed: 10617201]
- Selvin PR. Principles and biophysical applications of lanthanide-based probes. Annu Rev Biophys Biomol Struct. 2002; 31:275–302. [PubMed: 11988471]
- Mansoor SE, Palczewski K, Farrens DL. Rhodopsin self-associates in asolectin liposomes. Proc Natl Acad Sci U S A. 2006; 103:3060–3065. [PubMed: 16492772]
- 25. Zou P, Surendhran K, McHaourab HS. Distance measurements by fluorescence energy homotransfer: evaluation in T4 lysozyme and correlation with dipolar coupling between spin labels. Biophys J. 2007; 92:L27–29. [PubMed: 17142264]

 Taraska JW, Puljung MC, Zagotta WN. Short-distance probes for protein backbone structure based on energy transfer between bimane and transition metal ions. Proc Natl Acad Sci U S A. 2009; 106:16227–16232. [PubMed: 19805285]

- 27. Mansoor SE, McHaourab HS, Farrens DL. Mapping proximity within proteins using fluorescence spectroscopy. A study of T4 lysozyme showing that tryptophan residues quench bimane fluorescence. Biochemistry. 2002; 41:2475–2484. [PubMed: 11851393]
- Janz, JM. Biochemistry and Molecular Biology. Portland: Oregon Health and Science University;
 Structural Dynamics of Rhodopsin: Relationships Between Retinal Schiff Base Integrity and Receptor Signaling States; p. 312
- 29. Yao X, Parnot C, Deupi X, Ratnala VR, Swaminath G, Farrens D, Kobilka B. Coupling ligand structure to specific conformational switches in the beta2-adrenoceptor. Nat Chem Biol. 2006; 2:417–422. [PubMed: 16799554]
- Tsukamoto H, Farrens DL, Koyanagi M, Terakita A. The magnitude of the light-induced conformational change in different rhodopsins correlates with their ability to activate G proteins. J Biol Chem. 2009; 284:20676–20683. [PubMed: 19497849]
- 31. Janz JM, Farrens DL. Rhodopsin activation exposes a key hydrophobic binding site for the transducin alpha-subunit C terminus. J Biol Chem. 2004; 279:29767–29773. [PubMed: 15070895]
- 32. Tapley TL, Vickery LE. Preferential substrate binding orientation by the molecular chaperone HscA. J Biol Chem. 2004; 279:28435–28442. [PubMed: 15100228]
- Islas LD, Zagotta WN. Short-range molecular rearrangements in ion channels detected by tryptophan quenching of bimane fluorescence. J Gen Physiol. 2006; 128:337–346. [PubMed: 16940556]
- 34. Semenova NP, Abarca-Heidemann K, Loranc E, Rothberg BS. Bimane fluorescence scanning suggests secondary structure near the S3-S4 linker of BK channels. J Biol Chem. 2009
- Kosower EM, Kanety H, Dodluk H, Hermolin J. Bimanes. 9. Solvent and Substituent Effects on Intramolecular Charge-Transfer Quenching of the Fluorescence of syn-1,5,-Diazabicyclo[3.3.0]octadienediones (syn-9,10-Dioxabimanes). J. Phys. Chem. 1982; 86:1270– 1277.
- 36. Wang Y, Malenbaum SE, Kachel K, Zhan H, Collier RJ, London E. Identification of shallow and deep membrane-penetrating forms of diphtheria toxin T domain that are regulated by protein concentration and bilayer width. J Biol Chem. 1997; 272:25091–25098. [PubMed: 9312118]
- 37. Mansoor SE, McHaourab HS, Farrens DL. Determination of protein secondary structure and solvent accessibility using site-directed fluorescence labeling. Studies of T4 lysozyme using the fluorescent probe monobromobimane. Biochemistry. 1999; 38:16383–16393. [PubMed: 10587464]
- 38. Doose S, Neuweiler H, Sauer M. A close look at fluorescence quenching of organic dyes by tryptophan. Chemphyschem. 2005; 6:2277–2285. [PubMed: 16224752]
- Furstenberg A, Vauthey E. Excited-state dynamics of the fluorescent probe Lucifer Yellow in liquid solutions and in heterogeneous media. Photochem Photobiol Sci. 2005; 4:260–267.
 [PubMed: 15738993]
- 40. Kim T, Möller M, Winkler K, Alexiev U. A novel time-resolved fluorescence assay monitors how G-protein structural binding motifs evolve during receptor coupling (Abstract). Deutshe Gesellschaft für Biophysik. 2006
- 41. Mansoor, SE. Ph.D. Dissertation. Portland: Department of Biochemistry and Molecular Biology, Oregon Health & Science University; 2007. Site-Directed Fluorescence Spectroscopy: New Approaches for Studying Protein Structure and Oligomerization.
- 42. Marme N, Knemeyer JP, Sauer M, Wolfrum J. Inter- and intramolecular fluorescence quenching of organic dyes by tryptophan. Bioconjug Chem. 2003; 14:1133–1139. [PubMed: 14624626]
- 43. Pace, CN.; Scholtz, JM. Protein Structure: A Practical Approach. Creighton, TE., editor. Vol. Chapter 12. New York: Oxford University Press; 1997.
- 44. Becktel WJ, Schellman JA. Protein stability curves. Biopolymers. 1987; 26:1859–1877. [PubMed: 3689874]
- 45. Closs GL, Miller JR. Intramolecular Long-Distance Electron Transfer in Organic Molecules. Science. 1988; 240:440–447. [PubMed: 17784065]

46. Siders P, Cave RJ, Marcus RA. A model for orientation effects in electron-transfer reactions. J. Chem. Phys. 1984; 81:5613–5624.

- 47. Lakowicz, JR. Principles of fluorescence spectroscopy. 2nd ed., New York: Kluwer Academic/Plenum; 2006.
- 48. Spencer, RD. Ph.D. Dissertation. Department of Chemistry, University of Illinois at Urbana-Champaign; 1970. Fluorescence Lifetimes: Theory, Instrumentation, and Application of Nanosecond Fluorometry.
- 49. Barrio JR, Tolman GL, Leonard NJ, Spencer RD, Weber G. Flavin 1, N6-Ethenoadenine Dinucleotide: Dynamic and Static Quenching of Fluorescence. Proc. Natl. Acad. Sci. USA. 1973; 70:941–943. [PubMed: 4515004]



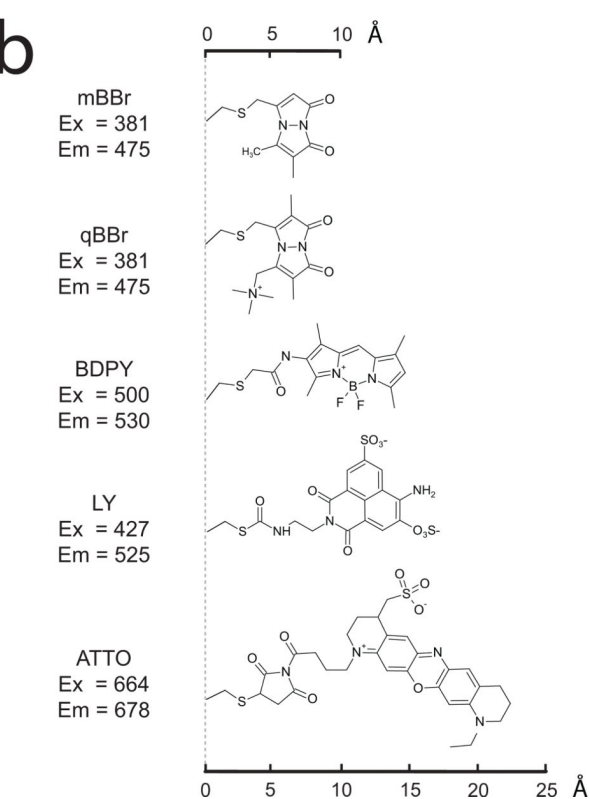


Figure 1. TrIQ sensitive fluorophores and their attachment sites on T4L (a) Model showing the location of the Trp (red) and the sites of fluorophore attachment (blue spheres at each C_{α} location). The $C_{\alpha}-C_{\alpha}$ distance from each site to the Trp are shown in parenthesis, and were calculated using coordinates from PDB 1L63. (b) The abbreviations, spectral properties and chemical structures of each cysteine-reactive, Trpsensitive fluorophore. The structures, drawn to the same scale, illustrate the differences in size and linker length for the various probes.

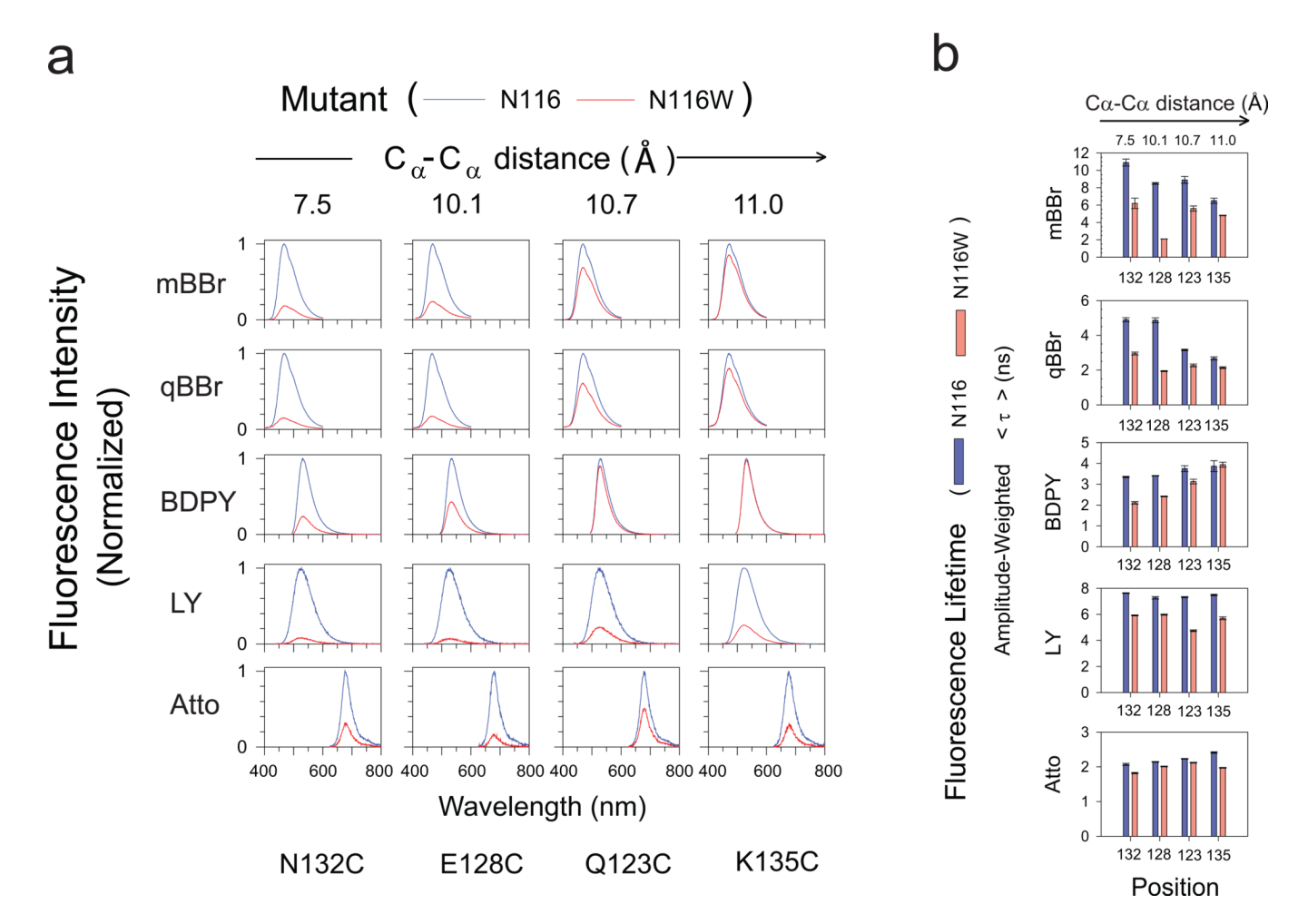


Figure 2. TrIQ effect on the fluorescence emission intensity and lifetime

The data are organized according to increasing probe size (top-to-bottom), and increasing distance from the Trp quencher (left-to-right). (a) Fluorescence emission spectra were taken for each TrIQ sensitive probe at the indicated sites on T4L, both with (red) and without (blue) the Trp at site 116. For all probes except Atto, the extent of TrIQ effect on emission decreases as a function of distance from the Trp. For each site/probe combination, the fluorophores' concentration was matched (for samples with and without the Trp) to enable direct assessment of the TrIQ effect. Then, to enable comparison between data, the spectra from each site/probe combination were normalized to the intensity of the Trp-less mutant (the N116 background mutant). (b) Results from fluorescence lifetime measurements of the same samples. The data are plotted as average amplitude-weighted fluorescence lifetime (<T>), both with (red) and without (blue) the Trp at site 116.

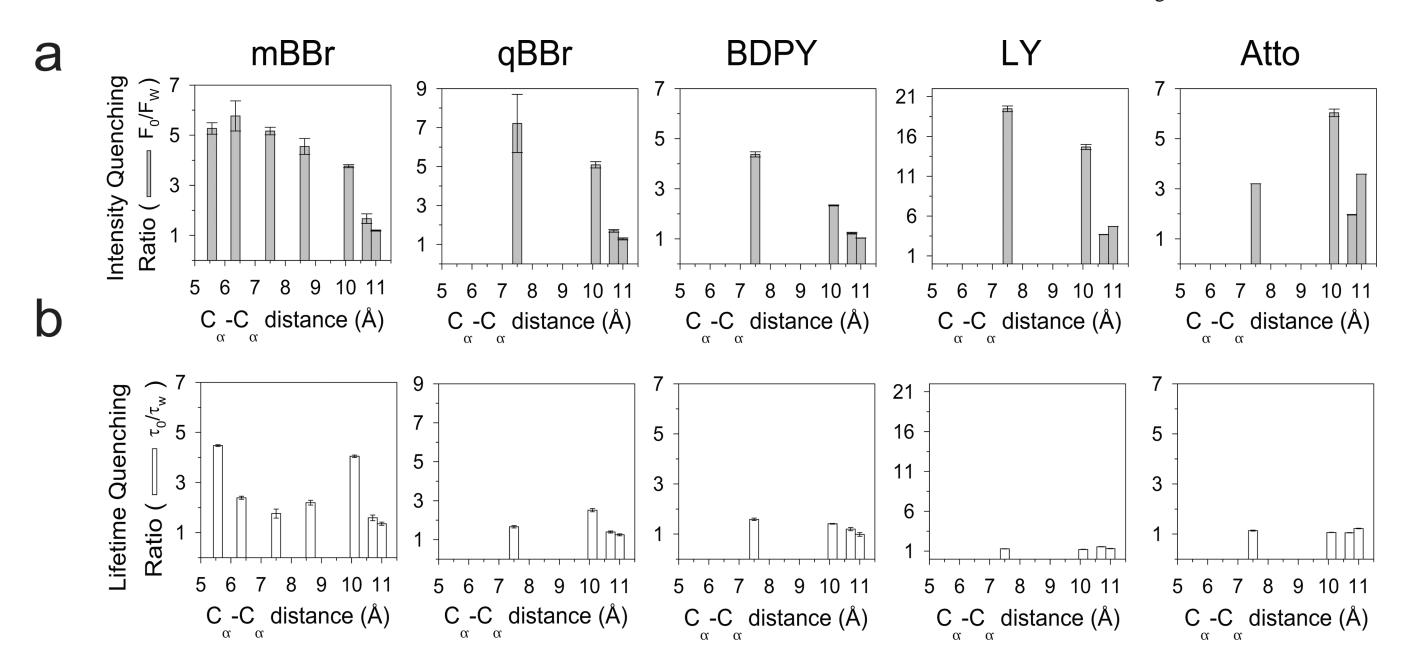


Figure 3. TrIQ affects emission intensity in a distance-dependence manner The distance-dependence of TrIQ can be assessed by plotting the "TrIQ ratio" vs. the distances separating the Trp and probe. A large ratio indicates substantial TrIQ, whereas a ratio of 1 indicates no TrIQ. (a) For the emission intensity data (F_0/F_w) , all probes show significant TrIQ at distances 10 Å. The smaller probes (mBBr, qBBr, BDPY) show less TrIQ as they move farther away from the Trp, and no quenching for C_α - C_α distance greater than 10 Å. In contrast, the larger probes (LY, Atto) show significant quenching over the entire range tested. These two probes thus display a larger "sphere of quenching". (b) Interestingly, the lifetime quenching ratios $(\langle \tau_0 \rangle/\langle \tau_w \rangle)$ do <u>not</u> show a clear distance-dependent pattern. In the absence of other factors, changes in the emission intensity should be mirrored in the lifetime, and thus F_0/F_w should equal $\langle \tau_0 \rangle/\langle \tau_w \rangle$. When they do not match, static quenching is indicated (see the text and Figure 4). The mBBr plot also includes data for three other C_α - C_α distances, taken from the Mansoor *et al*, 2002 study. These data represent C_α - C_α distances of 5.6 Å (mutants K124-B₁ and K124-B₁/W126F), 6.4 Å (mutants D72-B₁ and D72-B₁/R76W), and 8.6 Å (mutants L133-B1 and L133-B1/W138F).

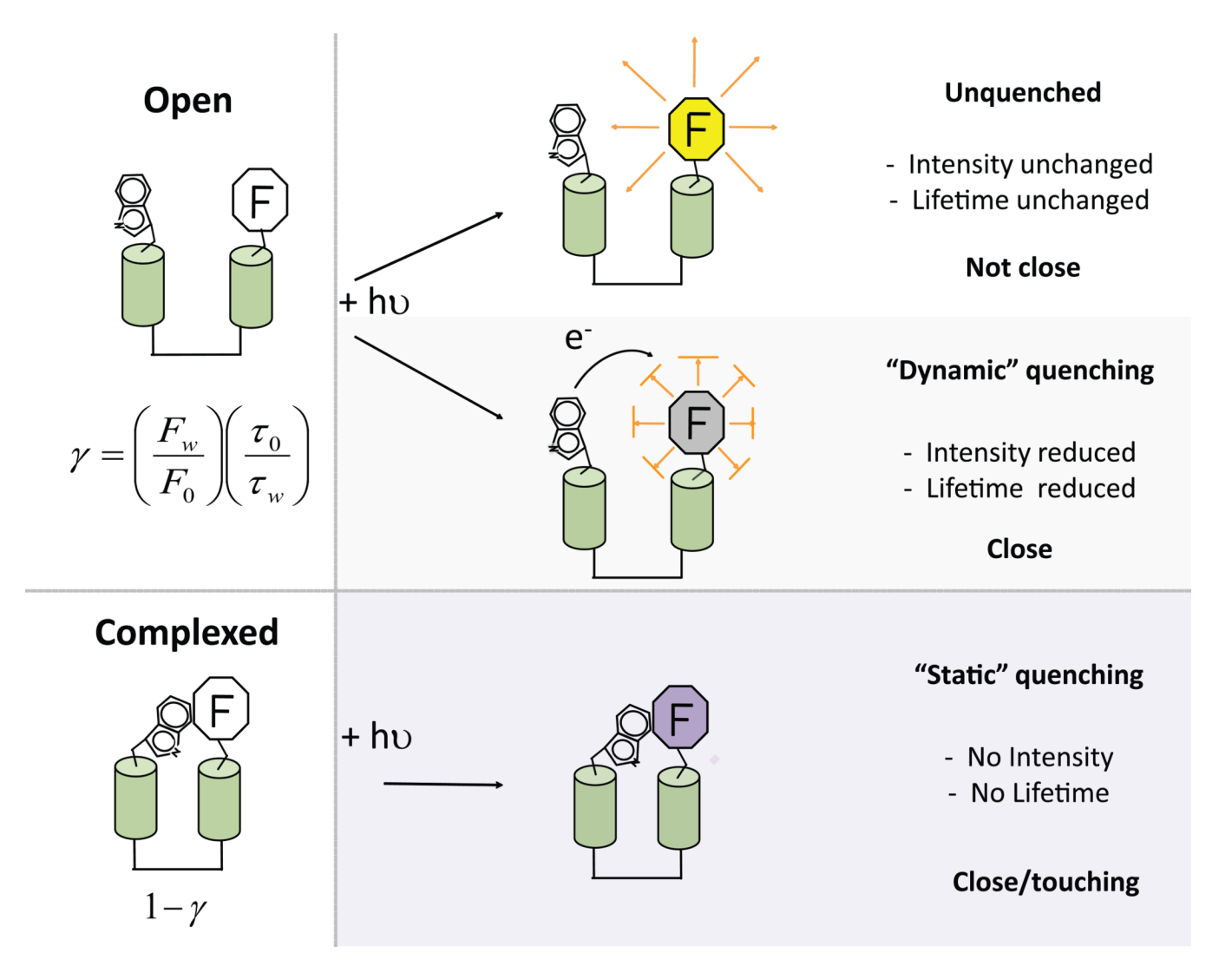


Figure 4. The fate of an excited fluorophore provides specific distance information in a TrIQ study

A probe in a TrIQ study can undergo three possible fates, and the fluorescence data can be analyzed to determine the relative fraction of probes in each. At larger separation distances, probes are in an "open" state, that is, they are not in contact with the Trp before light excitation. The fraction of "open" probes that never interact with the Trp will thus exhibit maximal fluorescence (illustrated as "Unquenched"). Some closer "open" probes can interact with the Trp at some time after excitation, and these will thus undergo "Dynamic quenching". A population of dynamically quenched probes has decreased fluorescence intensities and lifetimes, with the magnitude of decrease dependent on the amount of interaction. Of special interest are probes that are very close to the Trp, even before light excitation. If these probes contact the Trp and form a non-fluorescent complex (indicated in the figure as "Complexed"), they undergo static quenching, and thus do not contribute to the emission intensity or lifetime. Importantly, the relative fraction of probes in the open and complexed state can be determined from analysis of the fluorescence data. The fraction of probes in the open state, called γ , is readily extracted from the fluorescence data using the relationship $\gamma = (F_w/F_0)(\tau_0/\tau_w)$. In turn, the relative fraction of "complexed" probes, defined as probes in contact with Trp before excitation, is simply $(1-\gamma)$. These examples illustrate how, by simply comparing changes in fluorescence emission intensity with changes in the

fluorescence lifetime, one can extract information embedded in a TrIQ study that directly indicates if a probe is in contact with a Trp at the moment of light excitation. Probes in contact during the subnanosecond process of excitation are clearly "very close".

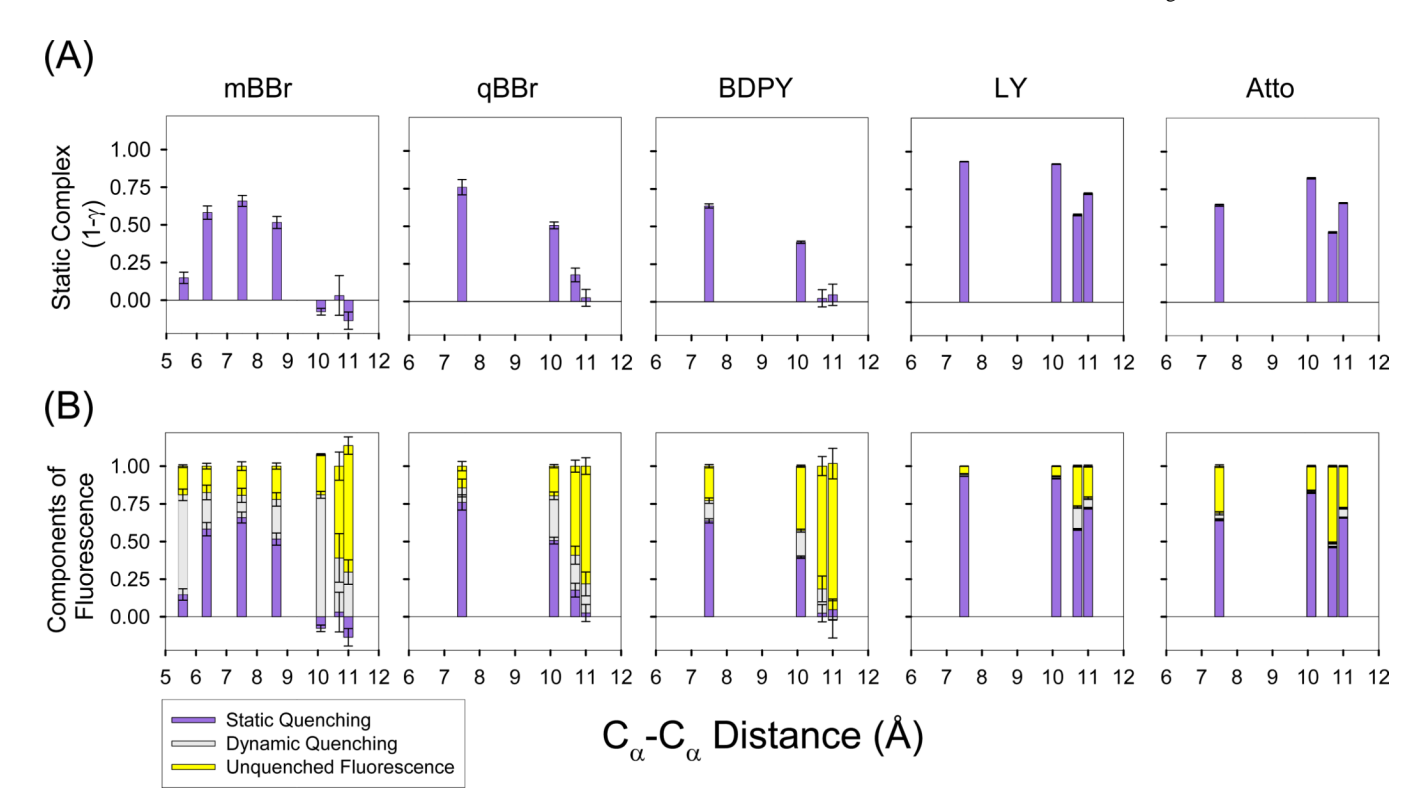


Figure 5. For smaller probes in a TrIQ study, Trp/fluorophore complex formation provides a quantifiable measure of close proximity

(A) The fraction of Trp/probe static complex formation plotted as a function of C_{α} - C_{α} distance from N116W clearly shows mBBr only exhibits static-complex formation with the Trp at distances less than ~ 10 Å. Interestingly, the larger probes show increasing amounts of Trp/fluorophore complex formation over longer distances, in a trend that correlates with the size of the probe and length of the attachment linker. These data indicate that each probe has a different "sphere of **static** quenching". Calculations were carried out described in the text and Figure 4. As with Figure 3, the plot for the mBBr data also include analysis of data from three other C_{α} - C_{α} distances reported in Mansoor *et al* 2002; at 5.6 Å, 6.4 Å and 8.6 Å. Derivations of gammaF and gammaDQ are provided in the Supporting Information.

(B) Total fluorescence signal is determined by the fraction of fluorophores which have formed a static ground-state complex with Trp, the fraction which are quenched dynamically by Trp, and the fraction that fluoresces without being quenched by either mechanism (see Supporting Information for more details). The fraction of fluorophores for which absorption occurs from an open, non-complexed conformation, (γ) , results in a fluorophore which can

emit the photon through unquenched fluorescence γ_F , where $\gamma_F = \left(\frac{\tau_w}{\tau_0}\right) \gamma$, yellow bars), or a fluorophore that can be quenched by a Trp residue through a dynamic quenching

mechanism (γ_{DQ} , where $\gamma_{DQ} = \left(1 - \frac{\tau_w}{\tau_0}\right) \gamma$, grey bars). The remaining fraction of total fluorophores, (1- γ), are quenched due to formation of a static, non-fluorescent complex at the moment of excitation, so called static quenching (purple bars). The pattern which emerges from this analysis shows that the smaller probes (the bimanes and BDPY) show a mixture of both dynamic and static quenching, but only at distances 10 Å, whereas the larger probes (LY and Atto) show mostly static quenching over the full range of distances tested. These behavior patterns define the "sphere of static quenching" and "sphere of

dynamic quenching" for each probe and should be taken into account when designing and interpreting TrIQ experiments. The error bars represent the S.E.M. for two data sets.